Polarimetric Features of Oyster Farm Observed by AIRSAR and JERS-1

Seung-Kuk Lee, *Student Member, IEEE*, Sang-Hoon Hong, *Student Member, IEEE*, Sang-Wan Kim, *Member, IEEE*, Yoshio Yamaguchi, *Fellow, IEEE*, and Joong-Sun Won, *Senior Member, IEEE*

***Abstract*—The polarimetric features of an oyster farm in a coastal area are analyzed to verify the applicability of radar polarimetry and interferometry. L-band Airborne Synthetic Aperture Radar (AIRSAR) data and Japan Earth Resources Satellite (JERS-1) data are used to examine the unique structure of an oyster farm located in South Korea. A specific feature of the oyster farm is the presence of numerous arrays of structures of various orientations that consist of exercise-bar-shaped poles protruding above sea level. This paper demonstrates that tide level is strongly correlated with the double-bounce scattering power from the vertical pole structures. This phenomenon is also verified by laboratory measurements using a network analyzer. In the laboratory experiment, double-bounce scattering and total power showed increasing trends with increased height of the vertical poles. Single-bounce scattering is sensitive to the orientation of horizontal poles relative to antenna orientation. HH-polarization is the most effective technique for imaging oyster farms from L-band polarimetric AIRSAR data. The authors were able to use a three-component decomposition of the AIRSAR data to distinguish an exposed tidal flat from a submerged tidal flat. The characteristics of the exposed tidal flat are similar to those of the carbon sponge in the laboratory test, except that the double-bounce scattering power is slightly greater in the real-world example. The single-bounce scattering component in AIRSAR data is generally greater than that in laboratory measurements because of sea-surface conditions and oyster growth. When the horizontal pole was aligned normal to the radar look direction, single-bounce scattering was greater than the double-bounce scattering, even under water-covered conditions. While a difference in tide height of 10 cm contributed approximately 3.0 dB in the laboratory experiment, a difference in tide height of 20 cm contributed to only approximately 1.7 dB in the JERS-1 SAR image intensity. JERS-1 SAR image intensity for areas dominated by double- and single-bounce scattering was 0.78 and 0.56, respectively. Results confirm that polarimetric SAR data are useful in selecting areas dominated by double-bounce scattering in oyster farms.**

***Index Terms*—Double-bounce scattering, L-band polarimetric Airborne Synthetic Aperture Radar (AIRSAR), radar polarimetry, single-bounce scattering, tide height.**

I. Introduction

POLARIMETRIC and interferometric radar observation have been attracting attention as a tool for environmental remote sensing of the Earth's surface. Alsdorf *et al.* [1], [2] successfully applied radar cross-interferometry to spaceborne L-band HH-polarization synthetic aperture radar (SAR) data to measure the water level in the Amazon. Radar signals that were double-bounced between the water surface and tree trunks produced coherent interferometric phases in the Amazon floodplain. Among various applications in terms of water–target interaction, attention has been drawn to oyster farms. Oyster farms have a unique structure that consists of many vertical poles fixed to the tidal flat and rising 1–2 m above the sea surface. An individual structural unit consists of a horizontal wooden pole across the top of two vertical poles, as shown in Fig. 1. An array of structural units forms an oyster farm block. The area that we have chosen to study is a section of Korean tidal seashore. The oyster farm structures are expected to show a correlation with polarimetric data. Therefore, the purpose of this paper is to retrieve information concerning the oyster farm from polarimetric SAR (PolSAR) data acquired by the Airborne SAR (AIRSAR) sensor and HH intensity of the Japan Earth Resources Satellite (JERS-1).

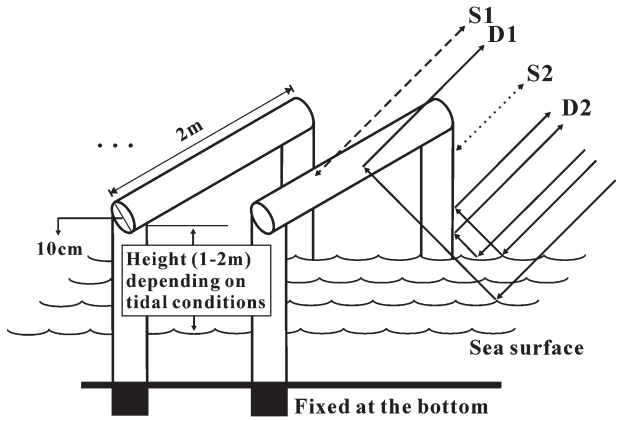

Fig. 1. Scattering in an oyster farm structure (S1: single-bounce scattering from a horizontal pole; S2: single-bounce scattering from a vertical pole; D1: double-bounce scattering from a horizontal pole; D2: double-bounce scattering from a vertical pole).

Kim *et al.* [3] reported that oyster farm structures behave as stable scatterers in the near coast and proposed an absolute phase reconstruction method using the combined information of the interferometric phase and a SAR intensity image. The radar measurements show a strong correlation with tide gauge data, yielding a correlation coefficient R^2 and root-mean-square error of 0.91 and 5.7 cm, respectively [3]. To reconstruct the absolute phase, wrapping counts were determined from SAR intensity images. It was assumed that the backscattered signals were dominated by double-bounce scattering between the water surface and poles from the oyster farm and that the backscattering power from the target was proportional to the

Manuscript received October 14, 2005; revised May 7, 2006. This work was supported by the Yonsei University Research Fund of 2004.

S.-K. Lee, S.-H. Hong, and J.-S. Won are with the Department of Earth System Sciences, Yonsei University, Seoul 120-749, Korea (e-mail: jswon@yonsei.ac.kr).

S.-W. Kim is with the Rosenstiel School of Marine and Atmospheric Science, University of Miami, Miami, FL 33149 USA.

Y. Yamaguchi is with the Department of Information Engineering, Niigata University, Niigata 950-2181, Japan.

Digital Object Identifier 10.1109/TGRS.2006.879107

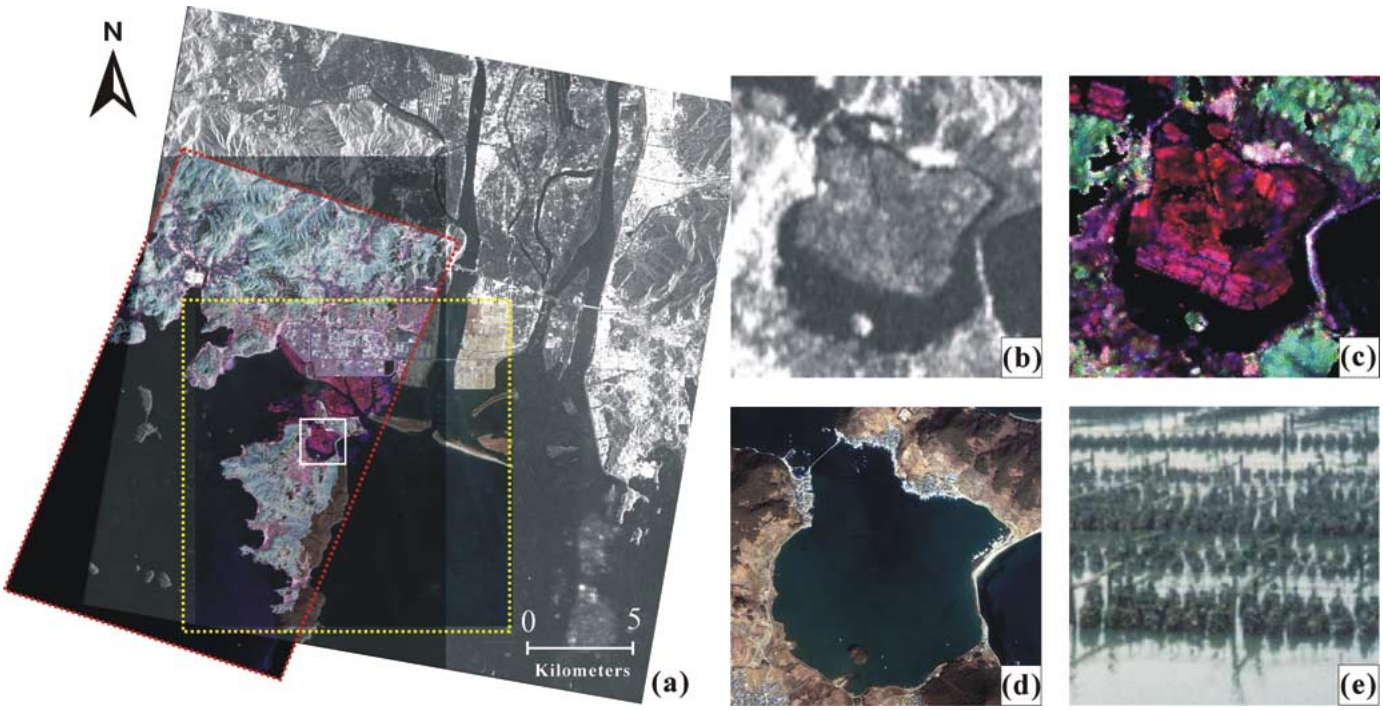

Fig. 2. (a) JERS-1 amplitude image of the study area overlaid with IKONOS (yellow square) and L-band AIRSAR images (red square). (b) Averaged JERS-1 amplitude image of the test site in Kaduckdo Bay. (c) AIRSAR PolSAR image of the test site. (d) IKONOS image of the test site. (e) Photograph of the oyster farms during winter.

exposed height of the vertical poles from the water surface, as seen in Fig. 1. Radar scattering in flooded forests of the Amazon has been examined using SIR-C polarimetry data [4]; however, the scattering mechanism in oyster farms has yet to be studied in detail. The assumptions made in [3] need to be reviewed from the perspective of radar polarimetry.

PolSAR is effective for understanding the target properties and backscattering mechanisms of a given target [5]. Various schemes have been developed for extracting the polarimetric properties of a target from PolSAR data. Van Zyl [6] proposed a three-component decomposition of PolSAR data by odd-bounce, even-bounce, and diffuse scattering. Another three-component scattering model was developed in [7], which describes the terrain by single-bounce scattering, double-bounce scattering, and volume scattering. Helix scattering power, which is especially effective for artificial objects, was added as a fourth component to the three-component model by Yamaguchi *et al.* [8]. Cloude and Pottier [9] introduced a PolSAR image classification scheme based on the polarimetric entropy H, anisotropy A, and eigenvector parameter α. In this paper, we examine a three-component scattering model of AIRSAR data and the backscattering intensity of JERS-1 data. Our decomposition scheme is based on the three-component scattering model proposed in [7].

This paper investigates the following two topics: 1) relationship between backscattering intensity and water level and 2) contribution of vertical and horizontal poles to double- and single-bounce scatterings. We selected those oyster farms suitable for tide height estimation by applying differential radar interferometry (DInSAR). To classify subareas of dominantly double-bounce and single-bounce scattering, we applied the Freeman decomposition method [7] to L-band NASA/JPL AIRSAR data obtained at the test site. Backscattering intensity models were finally tested using JERS-1 SAR data for subareas dominated by double-bounce and single-bounce scattering. The backscattering intensity models were then correlated with tide levels measured by a tide gauge. To confirm the test results and examine the detailed polarimetric nature of the vertical and horizontal poles, we carried out a laboratory experiment, using a scale model, in an anechoic chamber at Niigata University, Niigata, Japan.

This paper is organized in six sections. The test site is described in Section II. Laboratory measurements are presented in Section III. Section IV contains an analysis of AIRSAR data. JERS-1 image intensity is considered in Section V, and conclusions are presented in Section VI.

II. Description of the Test Site

The test site for this paper is located in Kaduckdo Bay, South Korea, which houses a number of oyster farms (Fig. 2). The site was previously used for a JERS-1 SAR test measuring tide levels [3]. The oyster farms of interest consist of arrays of 50–100 structural units; an individual unit consists of two vertical and one horizontal wood poles at 1–2 m above the water surface (Fig. 1). The diameter of each pole is approximately 10 cm. The vertical poles were secured into the tidal flat, with the section of poles exposed above sea level varying with tidal conditions. The horizontal poles are permanently above sea level and are oriented normal to the array direction.

Oyster farms were well imaged by spaceborne SAR [Fig. 2(b)] and AIRSAR [Fig. 2(c)]. The JERS-1 image in Fig. 2(a) is overlaid with IKONOS and L-band AIRSAR images. The JERS-1, AIRSAR, and IKONOS images of Kaduckdo Bay are shown in Fig. 2(b)–(d), respectively. The oyster

TABLE I
SYSTEM PARAMETERS FOR THE LABORATORY EXPERIMENT

Antenna	Rectangular horn
Polarization	HH, HV, VV
Frequency points	201
Wavelength	2.0 cm
Center frequency	15.0 GHz
Sweep frequency	14.0 - 16.0 GHz
Scanning points	64
Scanning interval	1.0 cm
Antenna height	146.0 cm
Incidence angle	45.0

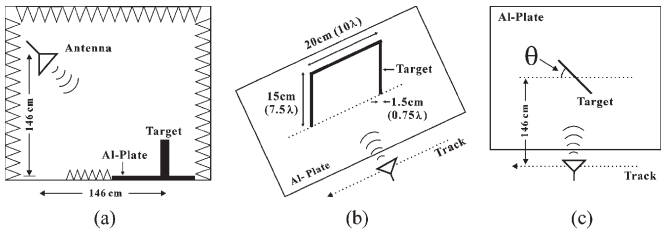

Fig. 3. Configuration of laboratory measurements. (a) Antenna and target geometry. (b) Target size. (c) Target orientation angle (θ), which is zero when the horizontal pole is oriented normal to the radar look direction.

farms are difficult to recognize in optic images, but are well imaged by SAR because of strong backscattering.

III. RADAR MEASUREMENTS IN THE LABORATORY

A. System Description and Measurements

To examine polarimetric backscattering behavior in detail, laboratory measurements were carried out within an anechoic chamber at Niigata University during January 2004 and January 2006. Some of the results from the experiments carried out in 2004 have already been published [10]; most of the results in this paper are data obtained in 2006. The experimental system consists of a vector network analyzer, polarized horn antennas, an antenna positioner, and a personal computer. System parameters are listed in Table I. The network analyzer was used to measure the scattering matrix. By scanning the polarimetric antenna set along a line by the positioner mounted on a rail, a synthetic aperture image was obtained. The azimuth-scanning interval was 1 cm (Table I).

Antenna and target configuration is shown in Fig. 3. The target orientation angle θ was set to zero when the horizontal pole was aligned normal to the antenna look direction, as shown in Fig. 3(c) [10]. Because the unit structure of the oyster farms does not have a typical polarimetric shape such as a dihedral, sphere, or wire, we simplified the target to a shape similar to that of an exercise bar (see Fig. 1). Because of the limited size of the laboratory, it was not possible to take measurements using a target structure of true size. Considering the wavelength of the AIRSAR L-band SAR system and the size of the actual oyster farming structure, the target size for the laboratory test was scaled down to approximately 1/10 that of the true size, and a Ku-band antenna was used. Although the ratio of microwave center frequency to target size was chosen to be as close as possible to the real-world example, the miniaturization of both the oyster farm structure and microwave center frequency might not exactly reflect real-world conditions. Instead of seawater and wet wooden poles, we used an aluminum plate and wooden sticks wrapped in aluminum tape. To simulate areas of exposed

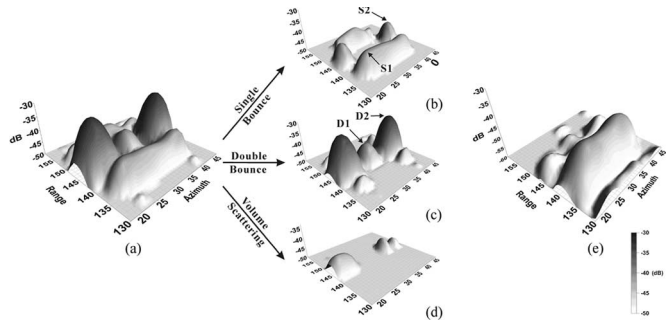

Fig. 4. Results of laboratory measurements for a standard unit target. (a) Three-dimensional total power tested with an aluminum plate at the base of the experiment. (b) Single-bounce scattering component (S1: single-bounce scattering from a horizontal pole; S2: single-bounce scattering from a vertical pole). (c) Double-bounce scattering component (D1: double-bounce scattering from a horizontal pole; D2: double-bounce scattering from a vertical pole). (d) Volume scattering component. (e) Results when the basal aluminum plate was replaced by carbon sponge. Note that the returned signals from vertical poles are greatly reduced in (e).

tidal flat, the aluminum plate was replaced by a carbon sponge. Scattering on the exposed tidal flat is dependent on factors such as grain size, surface water, soil moisture content, wavelength, and incidence angle and is therefore too complicated to reconstruct in the laboratory. Although the permittivity of the carbon sponge was not known, we used it to simulate the nonconductive conditions of the exposed tidal flat.

Fig. 3(b) depicts a standard target used in the experiment. Five vertical poles of different heights (10, 12.5, 15, 17.5, and 20 cm) were used to examine the effect of tide level on backscattering. We also took measurements at three different target orientation angles, i.e., 0°, 45°, and 90°. We repeated the measurements three times for each condition.

B. Measurement Results

Of a total of 64 $\times$ 1024 measured pixels, the 30 $\times$ 30 pixels immediately surrounding the target were meaningful. The HH-, HV-, and VV-components constituted a scattering matrix for each pixel, and the scattering matrix was averaged by a 3 $\times$ 3 subwindow. Freeman and Druden's three-component decomposition [7] was applied to the measured data sets.

Fig. 4(a) shows the total power from the standard target with an aluminum plate at the base. The target orientation angle in this case was 0°. Single-bounce, double-bounce, and volume scatterings are displayed in Fig. 4(b)–(d), respectively. There are three significant features of the radar returns, namely: 1) strong double-bounce scatterings from the two vertical poles (D2); 2) strong single-bounce scattering from the horizontal pole (S1); and 3) small double-bounce scattering from the horizontal pole (D1). As the single-bounce returns experienced shorter paths than the double-bounce returns, the single-bounce returns from the top horizontal pole imaged the front surfaces of the vertical poles. Double-bounce scattering was dominant from the vertical poles (80%), as shown in Table II, but single-bounce scattering (17%) was also significant. The horizontal pole produced the reverse result: single-bounce scattering was dominant (70%), followed by double-bounce scattering (30%), as listed in Table II. Fig. 5 shows that double-bounce scattering from the vertical pole is approximately -30.4 dB, whereas single-bounce scattering from the horizontal pole is approximately -40.8 dB. Thus, the double-bounce scattering

TABLE II
THREE-COMPONENT ANALYSIS OF RETURNED SIGNALS FROM THE STANDARD UNIT TARGET. PS: SINGLE-BOUNCE SCATTERING COMPONENT. PD: DOUBLE-BOUNCE SCATTERING COMPONENT. PV: VOLUME SCATTERING COMPONENT

	Ps(%)	Pd(%)	Pv(%)
Vertical pole	17	80	3
Horizontal pole	70	30	0

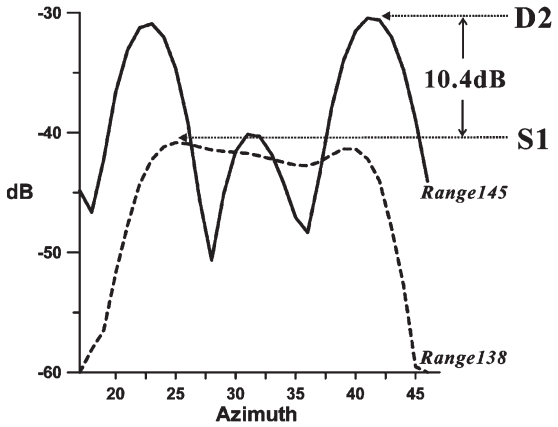

Fig. 5. Profiles along ranges of horizontal and vertical poles shown in Fig. 4(b) and (c). Single-bounce scattering from the horizontal pole is weaker than double-bounce scattering from the horizontal pole by 10.4 dB at zero target orientation angles (modified from [10, Fig. 5(b)]).

power from the vertical pole is stronger than the single-bounce scattering power by approximately 10.4 dB. This result is similar to that obtained in 2004 [10], and it indicates that double-bounce scattering from the vertical pole plays the most important role in backscattering from the unit target, even when the horizontal pole is aligned normal to the radar look direction.

Single-bounce scattering is significant from both the vertical and horizontal poles. This phenomenon suggests that the growth of oysters would increase the single-bounce scattering from the vertical pole. When the aluminum plate at the base of the experiment was replaced by a carbon sponge, the returns from the vertical poles were reduced significantly [Fig. 4(e)]. Consequently, the total power of the returned signals decreased. Although the bottom sediments of the tidal flat are not identical to the carbon sponge, this result indicates that double-bounce scattering from the vertical and horizontal poles decreases considerably when the poles are exposed to the air. AIRSAR data support the discussion to be described in the next section. Some oyster farms are located upon such intertidal flat, where tide levels cannot be measured by DInSAR.

We also investigated the influence of target orientation angle and target height on backscattering. Fig. 6(a) displays variations in total power and three components as a function of orientation angle. The total power decreased with increasing angle. Among the three components shown in Fig. 6(a), the single-bounce scattering component (Ps) decreased linearly, whereas the double-bounce scattering component (Pd) remained almost constant. The observed decrease in single-bounce scattering is the main contributor to the decrease in total power with increasing angle. This result indicates that the radar look direction relative to the orientation of the structure array is also important in terms of data acquisition.

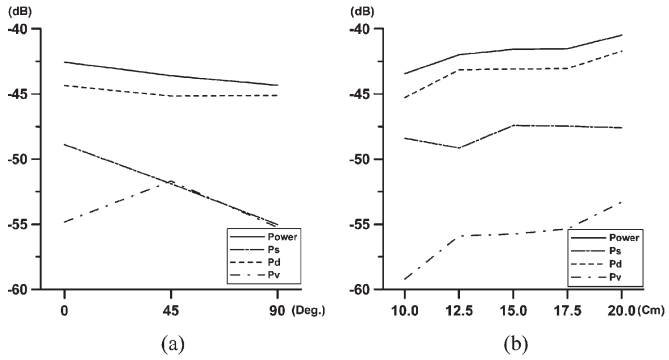

Fig. 6. Backscattering behavior according to (a) target orientation angles and (b) height of the vertical pole. The figure shows total power (solid line), single-bounce scattering (single dashed–dotted line), double-bounce scattering (dashed line), and volume scattering (double dashed–dotted line).

The exposed height of the vertical poles above the water surface varies with tidal conditions. Kim *et al.* [3] assumed a linear relation between JERS-1 SAR intensity image and tide level for absolute phase unwrapping. In this paper, we took measurements at five different vertical pole heights (10, 12.5, 15, 17.5, and 20 cm), and the results are presented in Fig. 6(b). Although total power did not show a linear trend, the total power generally increased with increasing pole height. The double-bounce scattering component in Fig. 6(b) shows an approximately straight line, with an average slope of 16.2°. While the increasing trend of the double-bounce scattering is similar to that of total power, single-bounce scattering did not increase with increasing pole height. The volume scattering component was also linear but lower than the double-bounce scattering by approximately 10 dB. Because of the limited number of pole heights and possible measurement errors, the results do not validate the linearity of the intensity image and water level. However, the SAR intensity image was used not for exact estimates of the water level but for determining the wrapping counts of the interferometric phase [3]. The near-linear pattern must be useful for this purpose, especially if regions dominated by double-bounce scattering are selected.

IV. ANALYSIS OF AIRSAR DATA

L-band PolSAR data were acquired on September 30, 2000, by NASA/JPL AIRSAR as part of the PACRIM-II experiment. The local time of data acquisition was 5:10 P.M., which was when the tide level was -50 cm above the lowest spring tide. Because the tide level was low, some parts of the tidal flat were exposed. The study area was covered by 1000 $\times$ 1000 pixels with a spatial resolution of 10 $\times$ 10 m. Polarimetry filtering developed by [11] was applied to the data to reduce speckle noise. Fig. 7(a) is a color composite image of the AIRSAR data. Because there were a number of vertical poles, we expected the strongest signal in VV-polarization. HH-polarization, however, produced the strongest returns from the oyster farm, as seen in Fig. 7(a). VV-polarization also imaged the oyster farm well but was slightly less effective than HH-polarization. A vegetated island was dominated by HV-polarization, in contrast to the part of the bay under aquaculture. This result suggests that L-band HH-polarization is best for observing oyster farms or similar structures located close to the coast using a single-polarization SAR system.

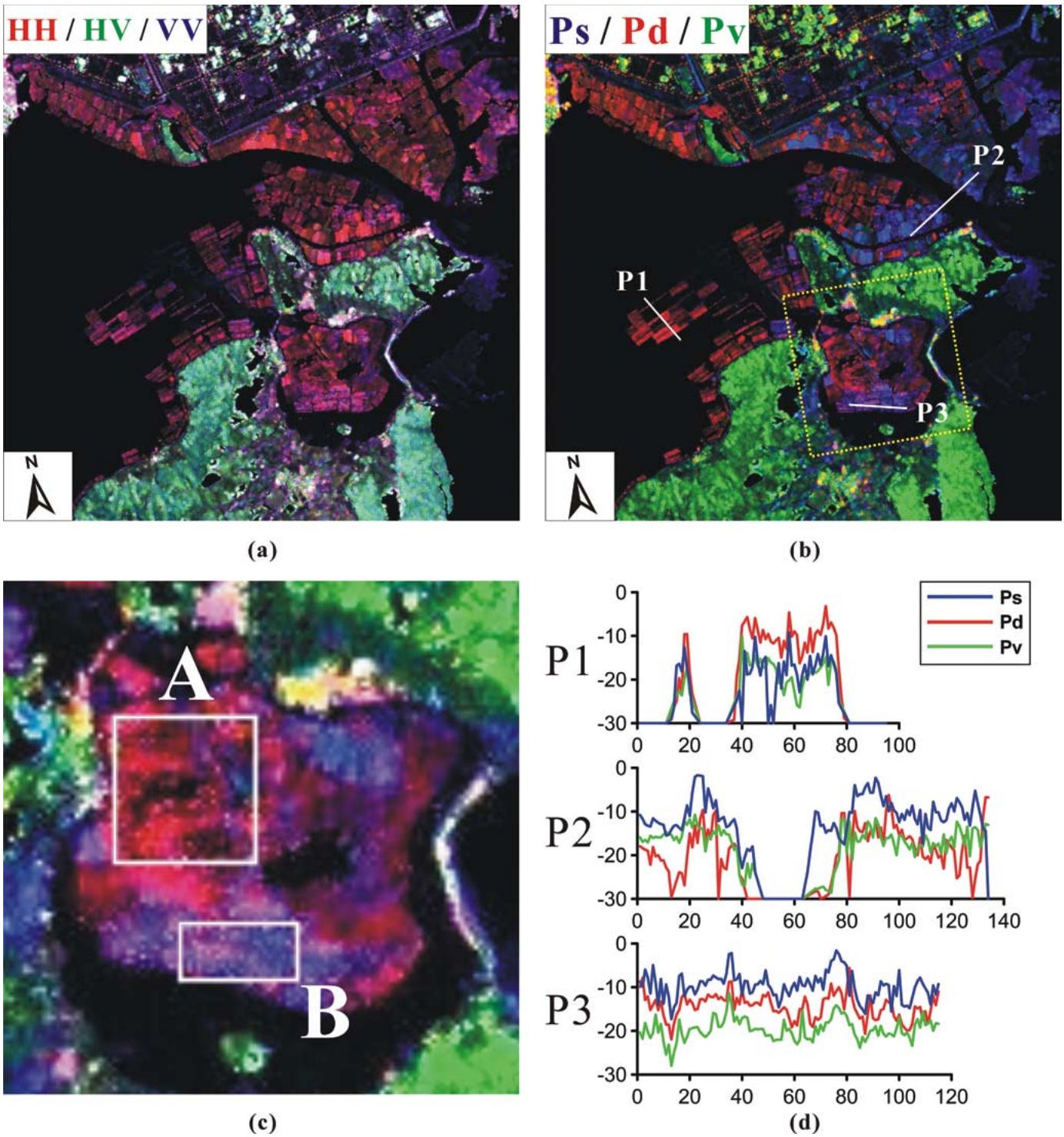

Fig. 7. L-band polarimetric AIRSAR images. (a) This false composite image was generated by assigning red, green, and blue to HH-, HV-, and VV-polarization, respectively (from [10, Fig. 12(b)]). (b) Three-component decomposed image of single-bounce scattering component Ps (blue), double-bounce scattering component Pd (red), and volume scattering component Pv (green) (from [10, Fig. 12(c)]). (c) Magnified three-component subimage of (b). Subareas A and B are oyster farms that are dominated by double- and single-bounce scattering, respectively. (d) Profiles of the three-component image along P1, P2, and P3 in (b).

The AIRSAR data were decomposed into single-bounce scattering, double-bounce scattering, and volume scattering by applying the method outlined in [7]. A color composite image of the three components is shown in Fig. 7(b). Volume scattering (green) dominated in the island but was insignificant in areas of oyster farms and tidal flat. Oyster farms were divided into two types, namely: 1) farms in the west and inside the bay area that are dominated by double-bounce scattering and 2) farms in the northeast that are dominated by single-bounce scattering. Water depth in the western parts of the tidal flat was generally greater than that of the eastern parts. From Fig. 7(b), it was possible to discriminate areas of exposed tidal flat from submerged areas. The areas dominated by double-bounce scattering are rendered in red in Fig. 7(b), which shows

TABLE III
NORMALIZED COMPONENTS OF SINGLE-BOUNCE SCATTERING (N_S), DOUBLE-BOUNCE SCATTERING (N_D), AND VOLUME SCATTERING (N_V) IN SUBAREA A AND B IN FIG. 7(c)

	Ns	Nd	Nv
Subarea A	0.28	0.50	0.22
Subarea B	0.65	0.24	0.11

a typical oyster farm where the tidal flat was covered with seawater.

The profiles of three components in the oyster farms shown in Fig. 7(d) display different polarimetric characteristics. Profile P1 in Fig. 7(d) shows strong double-bounce scattering, surpassing the single-bounce scattering and volume scattering. The volume scattering component is comparable to the single-bounce scattering, which contrasts with results from the laboratory experiment [Fig. 4(b)–(d)]. Oyster growth upon the vertical poles might help to increase volume scattering. In profile P2, the single-bounce scattering is dominant in oyster farms because of the effect of the exposed tidal flat sediment [blue areas in Fig. 7(b)]. This result is similar to the laboratory results when the bottom surface was covered with carbon sponge [Fig. 4(e)]. As the tidal flat surface is not completely absorbent and remnant surface water generally exists, double-bounce scattering does not disappear and is stronger than volume scattering, as shown in profile P2 in Fig. 7(d). Returns directly from the tidal flat sediments might have been mixed with signals from oyster farming structures.

The tidal flat with Kaduckdo Bay is rarely exposed to the air. Profile P3 in Fig. 7(d) shows an interesting feature. A typical oyster farm is standing above the water surface, but the single-bounce scattering is stronger than the double-bounce scattering. We first attempted to identify subareas within the bay that were dominated by double-bounce scattering and single-bounce scattering, where Kim *et al.* [3] had measured tide height by JERS-1 data. Normalized components were calculated using the following equation:

$$N_i = \frac{P_i}{P_S + P_D + P_V}, \qquad i = S, D, V. \tag{1}$$

If a certain N_i has a value larger than 0.5 in a subarea, the component i is considered as the dominant scattering. Subareas A and B in Fig. 7(c) were selected for the normalized component calculation. The results are summarized in Table III. N_D in subarea A was 0.5; therefore, double-bounce scattering was dominant. The single-bounce scattering component N_S was slightly larger than half of the N_D. Conversely, subarea B was dominated by single-bounce scattering with an N_S value of 0.65. Double-bounce scattering was about 37% of single-bounce scattering in this subarea.

The directions of horizontal poles along profile P3 were normal to the radar look direction. An aerial photo at a 1 : 37 500 scale was taken on February 18, 2000, and was reviewed to determine the direction of the array. The orientations of the horizontal poles in subareas A and B [Fig. 7(c)] were measured from the aerial photograph and plotted (Fig. 8). The orientations in subarea A were scattered but generally aligned in two directions, i.e., 0° and 80° E from the north. Oyster farms in subarea B were aligned approximately 20° E from the north, close to the AIRSAR azimuth (Fig. 8). As the radar look direction was almost normal to the orientations of horizontal poles, backscattering from the horizontal poles contributed significantly to the total power. Subarea B was the case in the laboratory experiment with zero target orientation angle, as shown in Figs. 4(a) and 5. In the laboratory measurements, double-bounce scattering was greater than single-bounce scattering by 10.4 dB. However, profile P3 in Fig. 7(d) of AIRSAR data shows that single-bounce scattering is greater than double-bounce scattering. In the laboratory measurement, single-bounce scattering directly from the submerged tidal flat (flat and polished aluminum plate) and the vertical poles (wrapped with aluminum tape) was minimized. In the real world, additional sources of single-bounce scattering include oysters growing on the vertical poles and uneven sea surface. Our results indicate that the orientations of the horizontal poles relative to the radar look direction is an important controlling factor of the backscattering mechanism, and that the orientation effect is more significant than that indicated by the laboratory measurements. Subareas A and B were selected to measure JERS-1 backscattering intensity, as described in the following section.

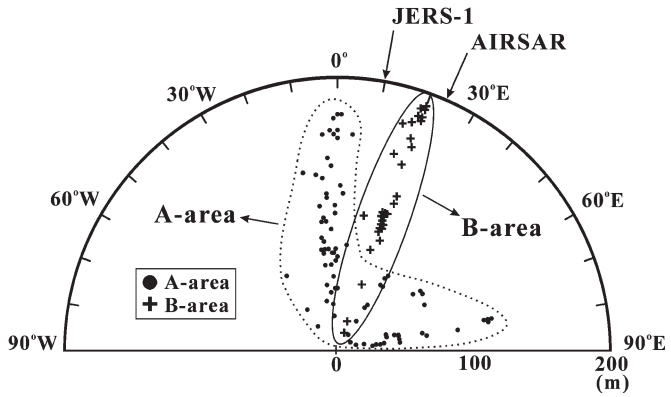

Fig. 8. Orientation of the sea farm estimated from an aerial photograph and azimuths of AIRSAR and JERS-1. The radius of the diagram represents the length of the sea farm array.

V. JERS-1 IMAGE INTENSITY

As oyster farming structures have changed little since the early 1990s, temporal differences between AIRSAR and JERS-1 observations were not a serious problem for subarea selection. The image intensity of the sea farms varies with factors such as date, tide, and sea-surface conditions.

The backscattering coefficient σ^0 of the JERS-1 SAR images was given by

$$\sigma^0 = 10 \log \overline{I} + CF, \qquad \text{where } \overline{I} = \frac{\sum DN^2}{N} \tag{2}$$

where $\overline{I}$ is the average pixel intensity, DN is the digital number of the amplitude image, N is the number of pixels, and CF is a radiometric calibration factor (-63.0 dB) [3]. The average σ^0 for each data set was first estimated for normal seas at three different sites. Radar backscattering from the normal sea surface recorded by JERS-1 SAR was relatively consistent (approximately -20 dB). The difference in radar backscattering for the three sites under normal sea conditions had to be less than 1 dB to be considered for further analysis. To ensure that the tidal flat was submerged, we only selected JERS-1

TABLE IV
LIST OF THE REMOTE SENSING DATA USED IN THIS PAPER

No.	System	Date (yyyy/mm/dd)	Tide level (cm)
1	JERS-1	1996/05/02	-26.0
2		1996/10/25	-27.0
3		1997/01/21	-15.0
4		1997/06/02	-46.0
5		1997/10/12	-46.0
6		1997/11/25	-20.0
7		1998/01/08	-31.0
8		1998/02/21	-4.0
9		1998/05/20	-32.0
10		1998/07/03	-6.0
11	AIRSAR L-band	2000/09/30	-50.0
12	Aerial Photo	2000/02/18	-77.0

data sets that were acquired when tide levels were higher than those during acquisition of the AIRSAR data. Ten JERS-1 SAR data sets satisfied the conditions required for further analysis. Tide levels at the timing of each JERS-1 SAR data acquisition are listed in Table IV. The flight directions of AIRSAR and JERS-1 differed by approximately 14°, as evident in Fig. 8.

Two models of JERS-1 image intensity for the oyster farms in subareas A and B were obtained as a function of sea level (Fig. 9). The open circles and crosses in Fig. 9 represent, respectively, the obtained values from subarea A, where bounce scattering is dominant, and from subarea B, where single-bounce scattering is dominant. JERS-1 SAR image intensities in subarea A are relatively well correlated with tide levels. The model estimated from the area dominated by double-bounce scattering (solid line) has a correlation coefficient R^2 of 0.78, whereas the value from the area dominated by single-bounce scattering (dashed line) is 0.56. As already evident from the laboratory test [Fig. 6(b)], the double-bounce scattering component shows a stronger correlation with sea level (i.e., exposed height of vertical poles). The laboratory test slightly overestimated the effect of variation in water level. In Fig. 6(b), the total power decreased by 3.0 dB because of a 10-cm difference in the height of exposed poles. The 20-cm difference in tide height shown in Fig. 9 contributed to an approximately 1.7-dB drop in total power in the JERS-1 SAR image. Even the image intensity in subarea A did not show an ideally linear relationship with sea level because radar backscattering in the area is a function of sea-surface conditions, oyster growth, and relative radar look direction in addition to water level. As the number of data points is limited to ten available data sets, it was difficult to make a meaningful linear regression or draw conclusions. However, the result is sufficient to demonstrate the importance of selecting subareas within a given test site that are dominated by double-bounce scattering when measuring sea level via the DInSAR technique.

VI. SUMMARY AND CONCLUSION

Radar polarimetry in oyster farms has not been extensively studied in the past. In this paper, we carried out laboratory tests, analysis of L-band AIRSAR full polarization data, and image intensity modeling of JERS-1 correlated with sea level. In the laboratory measurements, vertical poles contributed most to the backscattering. The total power from the vertical pole was 10.4 dB larger than that from the horizontal pole. Backscattering from the horizontal pole was also sensitive to the pole orientation relative to the radar look direction. Double-bounce scattering was a good indicator of the height of the vertical pole. When the experiment base was replaced with an absorber, single-bounce scattering from the horizontal pole was the most significant backscattering mechanism. The results obtained from the laboratory test were then used to interpret the L-band polrimetric AIRSAR data. AIRSAR data showed that L-band HH-polarization is the most effective method for observing oyster farms, followed by VV-polarization. From the AIRSAR three-component image, exposed tidal flat was successfully distinguished from submerged areas. Double-bounce scattering under exposed tidal flat conditions was greater than that measured in the laboratory. In the real world, single-bounce scattering is also significant, depending on certain factors such as sea-surface conditions and oyster growth. When the direction of the horizontal pole was approximately normal to the radar look direction, single-bounce scattering was greater than double-bounce scattering.

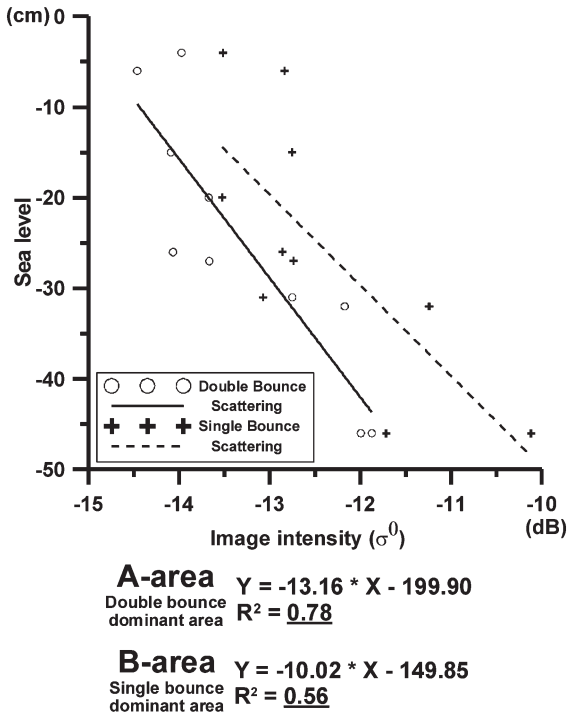

Fig. 9. SAR image intensity models as a function of sea level in areas dominated by double-bounce scattering (solid line) and single-bounce scattering (dashed line). Subareas A and B in Fig. 7(c) were used for the estimation.

Using the AIRSAR three-component image, we successfully discriminated subareas dominated by double-bounce scattering from oyster farms in the test site that were dominated by single-bounce scattering. Our JERS-1 image intensity model showed a correlation with water level, with R^2 values of 0.78 and 0.56 in subareas dominated by double- and single-bounce scattering, respectively. The variation in total power with changing water level was smaller than that determined in the laboratory experiment. Although the SAR intensity image does not have an ideally linear relationship with water level, the result suggests that it is important to select oyster farms that are dominated by double-bounce scattering when measuring sea

level by spaceborne DInSAR. In this paper, radar polarimetry was applied to review the relationship between water level and radar backscattering for absolute phase unwrapping. The contrasting polarimetric behaviors of vertical and horizontal poles indicate that it may be possible to apply PolSAR interferometry to water-level measurement using structures similar to those employed in oyster farms.

ACKNOWLEDGMENT

The authors would like to thank the NASA(JPL) AIRSAR/MASTER team and W. M. Moon for the AIRSAR image data. The authors also thank W. M. Boerner for the editorial correction of this paper.

REFERENCES

[1] D. E. Alsdorf, J. M. Melack, T. Dunne, L. A. K. Mertes, L. L. Hess, and L. C. Smith, "Interferometric radar measurements of water level changes on the Amazon flood plain," *Nature*, vol. 404, no. 6774, pp. 174–177, Mar. 2000.

[2] D. E. Alsdorf, L. C. Smith, and M. Melack, "Amazon floodplain water level changes measured with interferometric SIR-C radar," *IEEE Trans. Geosci. Remote Sens.*, vol. 39, no. 2, pp. 423–431, Feb. 2001.

[3] S.-W. Kim, S.-H. Hong, and J.-S. Won, "An application of L-band synthetic aperture radar to tide height measurement," *IEEE Trans. Geosci. Remote Sens.*, vol. 43, no. 7, pp. 1472–1478, Jul. 2005.

[4] L. L. Hess, J. M. Melack, S. Filoso, and Y. Wang, "Delineation of inundated area and vegetation along the Amazon floodplain with the SIR-C synthetic aperture radar," *IEEE Trans. Geosci. Remote Sens.*, vol. 33, no. 4, pp. 896–904, Jul. 1995.

[5] W.-M. Boerner, H. Mott, E. Luenburg, C. Livingstone, B. Brisco, R. J. Brown, and J. S. Patterson, "Polarimetry in radar remote sensing: Basic and applied concepts," in *Principles and Applications of Imaging Radar, Manual of Remote Sensing*, 3rd ed, vol. 2. F. M. Henderson and A. J. Lewis, Eds. New York: Wiley, 1998, pp. 272–357.

[6] J. J. van Zyl, "Unsupervised classification of scattering behavior using radar polarimetry data," *IEEE Trans. Geosci. Remote Sens.*, vol. 27, no. 1, pp. 36–45, Jan. 1989.

[7] A. Freeman and S. L. Durden, "A three-component scattering model for polarimetric SAR data," *IEEE Trans. Geosci. Remote Sens.*, vol. 36, no. 3, pp. 969–973, May 1998.

[8] Y. Yamaguchi, T. Moriyam, M. Ishido, and H. Yamada, "Four-component scattering model for polarimetric SAR image decomposition," *IEEE Trans. Geosci. Remote Sens.*, vol. 43, no. 8, pp. 1699–1706, Aug. 2005.

[9] S. R. Cloude and E. Pottier, "An entropy based classification scheme for land application of polarimetric SAR," *IEEE Trans. Geosci. Remote Sens.*, vol. 35, no. 1, pp. 68–78, Jan. 1997.

[10] S.-K. Lee, S.-H. Hong, and J.-S. Won, "Study of scattering mechanism in oyster farm by using AIRSAR polarimetric data," *Korean J. Remote Sens. (Korean ed.)*, vol. 21, no. 4, pp. 303–316, 2005.

[11] J. S. Lee, R. W. Jansen, M. R. Grunes, and G. D. Grandi, "Polarimetric SAR speckle filtering and its implication for classification," *IEEE Trans. Geosci. Remote Sens.*, vol. 37, no. 5, pp. 2363–2373, Sep. 1999.

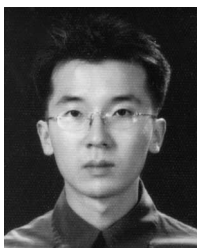

Seung-Kuk Lee (S'05) received the B.S. and M.S. degrees in Earth system sciences from Yonsei University, Seoul, Korea, in 2000 and 2005, respectively.

He is currently a Research Scientist at the Natural Science Research Institute, Yonsei University. His interests are in the field of PolSAR image analysis and interferometry.

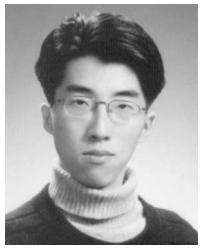

Sang-Hoon Hong (S'03) received the B.S. and M.S. degrees in geological sciences from Yonsei University, Seoul, Korea, in 1997 and 1999, respectively, where he is currently working toward the Ph.D. degree in radar remote sensing and geological sciences.

His research interests include radar interferometry, PolSAR, and raw signal processing.

Sang-Wan Kim (S'00–M'05) received the Ph.D. degree in Earth system sciences from Yonsei University, Seoul, Korea, in 2004. His Ph.D. dissertation was on the analysis of subsidence in urban areas using permanent scatterers and volcano monitoring using differential SAR interferometry.

His research interests include SAR data processing and the application of SAR interferometry to reclaimed coastal land and wetland. He was a Postdoctoral Research Scientist at Sejong University, Seoul. He is currently working as a Postdoctoral Researcher at the Center for Southeastern Tropical Advanced Remote Sensing, University of Miami, Miami, FL.

Yoshio Yamaguchi (M'81–SM'94–F'02) received the B.E. degree in electronics engineering from Niigata University, Niigata, Japan, in 1976, and the M.E. and Dr.Eng. degrees from the Tokyo Institute of Technology, Tokyo, Japan, in 1978 and 1983, respectively.

In 1978, he joined the Faculty of Engineering, Niigata University, where he is a Professor and the Head of the Information Engineering Department. From 1988 to 1989, he was a Research Associate at the University of Illinois at Chicago. His interests are in the field of radar polarimetry, microwave sensing, and imaging.

Dr. Yamaguchi is a member of the Institute of Electronics, Information and Communication Engineers of Japan. He served as Vice-Chair (2000–2001) and Chair (2002–2003) of the IEEE GRSS Japan Chapter, Organizer of PI-SAR Workshops (2000–2005) in Japan, and Associate Editor for Asian Affairs of the IEEE GRSS NEWSLETTER (since 2003).

Joong-Sun Won (S'92–M'93–SM'03) received the B.S. and M.S. degrees in geology and geophysics from Yonsei University, Seoul, Korea, in 1983 and 1985, respectively, and the Ph.D. degree in geophysics from the University of Manitoba, Winnipeg, MB, Canada, in 1993.

From 1993 to 1996, he was a Senior Scientist with the Marine Geology Division, Korea Ocean Research and Development Institute. He is currently an Associate Professor with the Department of Earth System Sciences, Yonsei University. His research interests include remote sensing, tidal flats, geohazard, signal processing, and radar interferometry.